Template-free synthesis of urchin-like Co_3O_4 hollow spheres with good lithium storage properties

Xianhong Rui [a,b], Huiteng Tan [a], Daohao Sim [a], Weiling Liu [a], Chen Xu [a], Huey Hoon Hng [a], Rachid Yazami [a], Tuti Mariana Lim [b,c,**], Qingyu Yan [a,d,e,*]

[a] School of Materials Science and Engineering, Nanyang Technological University, 639798 Singapore, Singapore
[b] School of Civil and Environmental Engineering, Nanyang Technological University, 639798 Singapore, Singapore
[c] School of Life Sciences and Chemical Technology, Ngee Ann Polytechnic, 599489 Singapore, Singapore
[d] Energy Research Institute, Nanyang Technological University, 637459 Singapore, Singapore
[e] TUM CREATE Centre for Electromobility, Nanyang Technological University, 637459 Singapore, Singapore

HIGHLIGHTS

► Hierarchical urchin-like Co_3O_4 hollow spheres are successfully synthesized.
► A plausible mechanism for the formation of urchin structures is proposed.
► Such Co_3O_4 exhibits excellent high-rate capability and cycling stability.

ARTICLE INFO

ABSTRACT

Hierarchical urchin-like hollow spheres (5—8 μm in diameter) assembled by one-dimensional nanowires consisting of many interconnected Co_3O_4 nanoparticles (10—50 nm) are successfully synthesized. $Co(CO_3)_{0.5}(OH) \cdot 0.11H_2O$ precursors are firstly prepared by a hydrothermal process. The morphological evolution process of $Co(CO_3)_{0.5}(OH) \cdot 0.11H_2O$ hollow urchin precursors is investigated and a plausible mechanism is proposed. Then, the $Co(CO_3)_{0.5}(OH) \cdot 0.11H_2O$ are converted to Co_3O_4 through heat treatment in air. As an anode material for lithium ion batteries, urchin-like Co_3O_4 hollow spheres exhibit highly reversible specific capacities, good cycling stabilities and excellent rate capabilities (e.g., 433 mAh g^{-1} at 10 C). The superior performances result from the synergetic effect of integral urchin-like microstructure, small diffusion lengths in the nanoparticle building blocks and sufficient void space to buffer the volume expansion.

1. Introduction

Cobalt oxide, Co_3O_4, an important magnetic p-type semiconductor, has attracted great attention for their potential applications in lithium-ion batteries (LIBs) [1—4], supercapacitors [5—8], gas sensing [3,9], catalysis [10—12] and electrochromic devices [13]. Owing to its high theoretical capacity of $\sim$890 mAh g^{-1} that is

about two times larger than that of the currently used graphite, Co_3O_4 is considered to be an attractive anode material for next-generation LIBs. Nevertheless, the practical use of this material is still hindered by the rapid capacity fading upon extended cycling and/or poor rate capability due to the large volume change during repeated lithium uptake and removal reactions and its low electronic conductivity. To alleviate these problems, one effective strategy is to prepare nanometer-sized materials with designed hierarchical structures [1,14—18]. It is mainly due to that such structures offer both advantages of nanostructured building blocks and micro- or submicrometer-sized structures. The nanoscale building blocks can provide large interfacial contact area and short Li^+ transport distance, leading to better rate capabilities [19—28]. The void space in the hierarchical nanostructures can buffer the huge volume changes during the lithium insertion/extraction process and alleviate the pulverization of the electrode material,

* Corresponding author. Nanyang Technological University, School of Materials Science and Engineering, Block N4.1 Nanyang Avenue, Singapore 639798, Singapore. Tel.: +65 6790 4583; fax: +65 6790 9081.
** Corresponding author. School of Civil and Environmental Engineering, Nanyang Technological University, 639798 Singapore, Singapore. Tel.: +65 6790 4583; fax: +65 6790 9081.
E-mail addresses: XHRUI@ntu.edu.sg (X. Rui), tmlim@ntu.edu.sg (T.M. Lim), Alexyan@ntu.edu.sg (Q. Yan).

which is beneficial for improving the cycling stability [29]. Moreover, the cavities in the hierarchical nanostructures may offer extra space for the lithium storage, which results in enhanced specific capacities of the battery [30]. Up to now, although various morphologies of Co_3O_4, such as nanoparticles [31], nanorods/-wires/-tubes [3,32–34], nanosheets/-discs/-platelets, nanocubes and hierarchical nanoflowers or more complex structures [5,35–41] have been synthesized, controlling the assembly of low-dimensional Co_3O_4 building units into hollow structures is still a challenge.

Herein, hierarchical urchin-like Co_3O_4 hollow spheres are obtained by a simple and environmentally friendly approach. $Co(CO_3)_{0.5}(OH) \cdot 0.11H_2O$ hollow urchin structures were prepared by a hydrothermal process. We propose a formation mechanism for $Co(CO_3)_{0.5}(OH) \cdot 0.11H_2O$ hollow structures based on the Ostwald ripening processes. These $Co(CO_3)_{0.5}(OH) \cdot 0.11H_2O$ are converted to Co_3O_4 urchin structures through a heat treatment. As an anode material for LIBs, the Co_3O_4 hollow urchins can deliver high specific capacities with stable cycling performance, especially at high C rates (*e.g.*, 433 mAh g^{-1} at 10 C).

2. Experimental

2.1. Synthesis of urchin-like Co_3O_4 hollow spheres

In a typical synthesis, 1 mmol of $Co(NO_3)_2 \cdot 6H_2O$, 3 mmol of NH_4F, and 5 mmol of $CO(NH_2)_2$ were dissolved in 35 mL of deionized water under vigorous stirring. The resultant homogeneous solution was then transferred to a Teflon lined stainless-steel autoclave (capacity of 50 mL). The autoclave was sealed and maintained at 120 °C for 5 h. After hydrothermal reaction, the autoclave was cooled to ambient temperature naturally, and pink products were collected by centrifugation follow by repeated washing with water and ethanol and then dried at 70 °C. Finally, the as-prepared precursors were calcined in air at 400 °C for 2 h with a heating rate of 5 °C min^{-1}.

2.2. Materials characterization

X-ray powder diffraction (XRD) patterns were recorded on a Bruker AXS D8 advance X-ray diffractometer using Cu Kα radiation. The morphology was investigated by using a field-emission scanning electron microscopy (FESEM) system (JEOL, Model JSM-7600F), and the nanostructure was characterized by using a transmission electron microscopy (TEM) system (JEOL, Model JEM-2010) operating at 200 kV.

2.3. Electrochemical measurements

The coin-type cells were assembled in an argon-filled glove-box, where both moisture and oxygen levels were less than 1 ppm. The working electrodes were fabricated by mixing of Co_3O_4, multi-walled carbon nanotubes and poly(vinyldifluoride) (PVDF) at a weight ratio of 70:20:10 in N-methylpyrrolidone (NMP) solvent and then pasting on the copper foils. The lithium foils were used as counter/reference electrodes and the electrolyte was a solution of 1 M LiPF$_6$ in ethylene carbonate (EC)/dimethyl carbonate (DMC) (1/1, w/w). The cells were tested on a NEWARE multi-channel battery test system with galvanostatic charge and discharge in the voltage range of 0.005–3.0 V.

3. Results and discussion

The phase purity of the products, obtained through the hydrothermal process at 120 °C for 5 h with a molar ratio of NH_4F:$Co(NO_3)_2$ ($I_{NH_4F:Co(NO_3)_2} = 3:1$), was characterized by the powder X-ray diffraction (XRD) technology (Supplementary data, Fig. S1a). All the diffraction peaks can be well indexed to the orthorhombic cobalt hydroxide carbonate, $Co(CO_3)_{0.5}(OH) \cdot 0.11H_2O$ (JCPDS card No. 48-0083). No peaks from other possible phases, such as $Co(OH)_2$ and $CoCO_3$, can be detected. The weak diffraction intensities indicate that the sample is not well crystallized. The low- and high-magnification field emission scanning electron microscopy (FESEM) images (Fig. 1a–c) show that the as-prepared $Co(CO_3)_{0.5}(OH) \cdot 0.11H_2O$ sample consists of uniform hierarchical urchin-like spheres with diameters of 5–10 μm, which are assembled from radially oriented 1D structures. Interestingly, seen from an incomplete sphere (Fig. 1d and inset in Fig. 1e), the core of this urchin-like assembly is hollow with typically 1–2 μm in diameter, and the building blocks (1D structures) are nanowires with typically lengths of 3–5 μm. A transmission electron microscopy (TEM) image taken from the edge of an urchin, as shown in Fig. 1e, suggests that these nanowires are needle-like with widths of 200–300 nm at the front part, ~100 nm at the middle part and 20–50 nm at the tip, indicating characteristic of the lateral growth during their formation. High-magnification TEM image (Fig. 1f) reveals that there are many nanopores of 2–8 nm in the nanowires. The high resolution (HR) TEM observation (Fig. 1g) indicates that the nanowires are single crystalline with the long axis of the nanowires oriented along <010> direction. The observed interfringe spacing of 0.88 nm corresponds well to the {100} planes of orthorhombic $Co(CO_3)_{0.5}(OH) \cdot 0.11H_2O$ (JCPDS card No. 48-0083).

To reveal the growth process of such interesting hierarchical urchin-like $Co(CO_3)_{0.5}(OH) \cdot 0.11H_2O$ hollow spheres, time-dependent experiments were carried out. At an early stage (reaction time = 2 h), numerous nanoparticles with sizes of 20–50 nm formed (Fig. 2a). After reaction for 3 h, solid spheres (~2 μm in diameter) with small nanorods on the surfaces were obtained (Fig. 2b). As the reaction time prolonged to 4 h, the spheres became larger (3–4 μm in diameter), and the nanorods on the surfaces grew longer and denser (Fig. 2c). In addition, the interior of spheres changes to hollow with typically ~400 nm in diameter (Fig. 2d). After 5 h, uniform urchin-like hollow spheres formed (Fig. 1a–b). Further increasing the reaction time to 6 h, we found that the urchin-like structure collapsed due to complete dissolution of inner core (Supplementary data, Fig. S2). On the basis of above observations, a plausible mechanism for the template-free synthesis of the $Co(CO_3)_{0.5}(OH) \cdot 0.11H_2O$ hollow urchins is proposed (Fig. 3). In the initial stages, many nanoparticles formed and spontaneously aggregated into large spheres to minimize the overall surface energy of the system. Subsequently, short nanorods were grown on the surfaces due to their propensity for one-dimensional growth [42,43]. As the reaction proceeded further, the inner core was dissolved to assist crystal growth of outer surface of short nanorods to large needle-like nanowires through Ostwald ripening.

Interestingly, when increased the $I_{NH_4F:Co(NO_3)_2}$ to 10:1, the morphologies of the precursors transformed from urchin-like hollow spheres to hexapods with sizes of 5–8 μm (Supplementary data, Fig. S1b for additional XRD and Fig. S3 for FESEM characterization), and the yield of the product is low. It is probably due to the corrosive behavior of the HF ($NH_4F + H_2O \rightarrow NH_3 \cdot H_2O + HF$) [44,45]. Excessive HF not only corrodes the $Co(CO_3)_{0.5}(OH) \cdot 0.11H_2O$ formed but also hinders the nucleation and crystal growth by forming $CoF_x^{(x-2)-}$ complexes [43].

Subsequent thermal treatment of urchin-like $Co(CO_3)_{0.5}(OH) \cdot 0.11H_2O$ hollow spheres in air at 400 °C for 2 h led to the formation of cobalt oxide, and its crystal structure was investigated by XRD (Fig. 4a). All the diffraction peaks can be indexed as cubic phase Co_3O_4 with a space group of *Fd3m* (JCPDS card no. 42-1467) [1]. No impurities, such as precursor compounds, have been detected. FESEM images (Fig. 4b–c) indicate that the urchin-like sphere
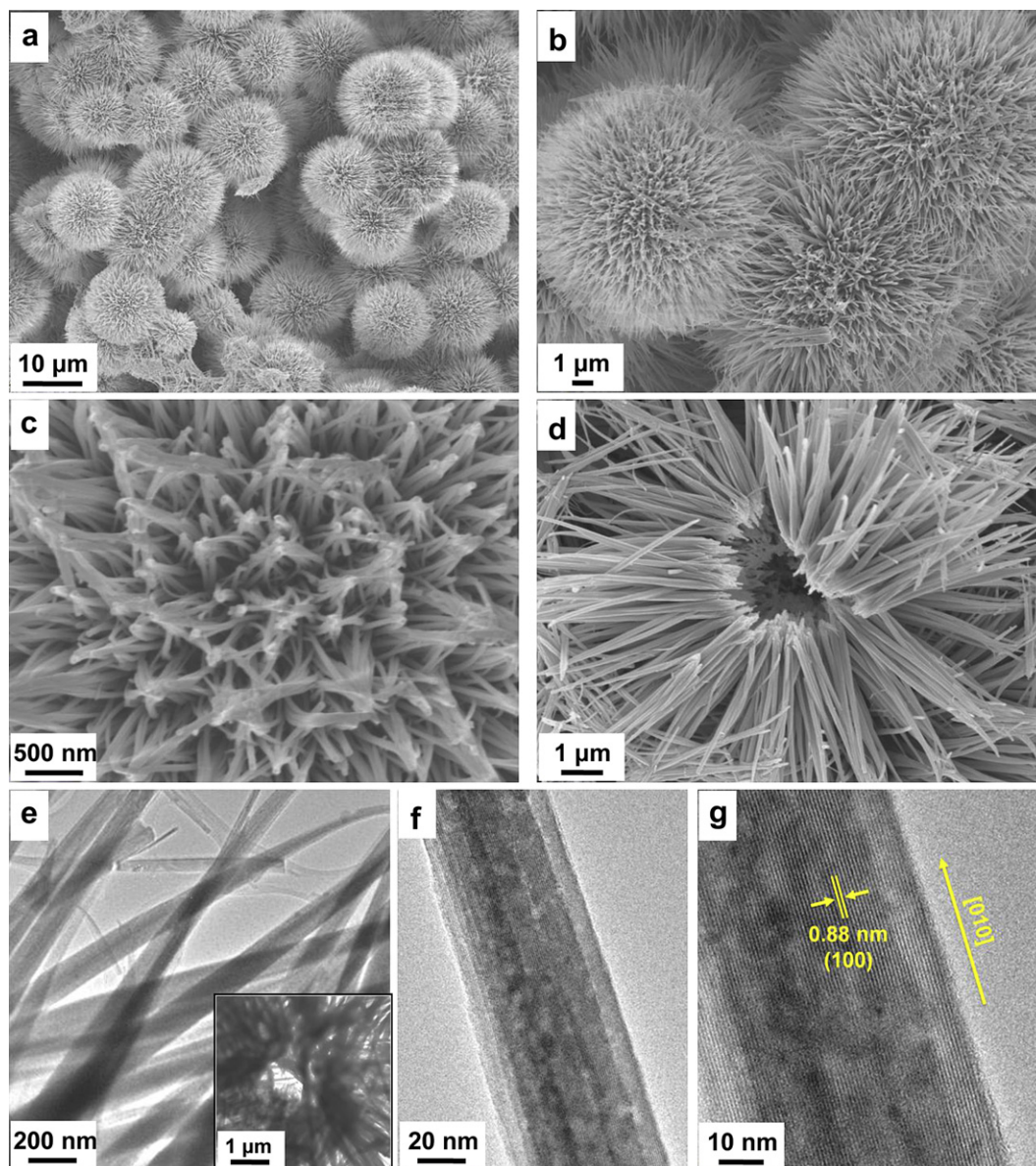
Fig. 1. (a–c) FESEM images at different magnifications for the hierarchical urchin-like $Co(CO_3)_{0.5}(OH)\cdot0.11H_2O$ spheres prepared with $I_{NH_4F:Co(NO_3)_2} = 3:1$. (d) An incomplete sphere showing a hollow interior. (e) A detailed TEM observation of the urchin-like sphere. (f) An individual nanowire of $Co(CO_3)_{0.5}(OH)\cdot0.11H_2O$ (TEM image). (g) An HR-TEM image of lattice fringes.

configuration of the precursors is retained during the thermal treatment process. As seen from low-magnification TEM image (Fig. 4d), the core of the urchin is still hollow. The magnified TEM images in Fig. 4e–f clearly indicate that each building block (Co_3O_4 nanowire) is composed of many interconnected Co_3O_4 nanocrystals with the sizes of 10–50 nm, resulting from the recrystallization process from $Co(CO_3)_{0.5}(OH)\cdot0.11H_2O$. These urchins were not destroyed even after half hour sonication process as illustrated by the TEM observation, suggesting that they are mechanically robust. The Co_3O_4 nanoparticles possess good crystallinity (Fig. 4g), displaying clear lattice fringes with a spacing of 0.46 nm, which is indexed to the {111} planes of Co_3O_4 crystals (JCPDS card no. 42-1467). Similarly, Co_3O_4 hexapods were obtained by thermal annealing of $Co(CO_3)_{0.5}(OH)\cdot0.11H_2O$ hexapod precursors (Supplementary data, Fig. S4).

To evaluate the Li-ion storage properties of the hierarchical urchin-like Co_3O_4 hollow spheres, a series of electrochemical measurements were carried out at room temperature based on a coin-type half cell configuration [46–48]. Fig. 5a shows galvanostatic charge–discharge voltage profiles of the urchin-like Co_3O_4 hollow spheres electrode between 0.005 and 3.0 V at a current density of 90 mA g^{-1} (0.1 C). The profiles are very similar to those reported previously [1], indicating the same electrochemical pathway. During the first discharge (Li$^+$ intercalation), there are two well-defined voltage plateaus at around 1.2 and 1.0 V, corresponding to the conversion of Co_3O_4 to an intermediate-phase CoO (or Li$_x$Co$_3$O$_4$) and then to metallic Co, respectively (i.e., $Co_3O_4 + 8Li^+ + 8e^- \rightarrow 4Li_2O + 3Co$) [1]. The first discharge capacity is ~1420 mAh g^{-1} with a contribution of about 810 mAh g^{-1} from above plateau region, which is comparable to the theoretical capacity of Co_3O_4 (890 mAh g^{-1}). The extra capacity (~610 mAh g^{-1}) mainly comes from low-voltage region (below 1 V), which is usually ascribed to irreversible reactions (e.g., decomposition of electrolyte) to form a solid electrolyte interphase
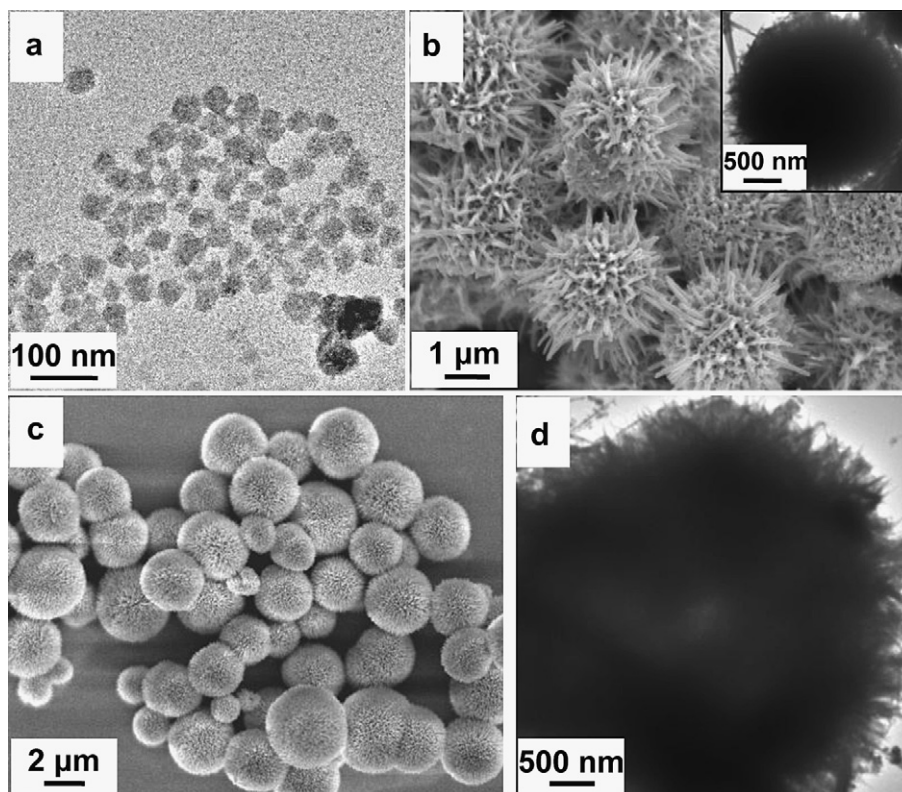
Fig. 2. Morphological evolution of the hierarchical urchin-like $Co(CO_3)_{0.5}(OH)\cdot 0.11H_2O$ spheres prepared at 120 °C after different reaction times: 2 h (a), 3.0 h (b), and 4.0 h (c–d).

(SEI) layer and possibly interfacial lithium storage (*e.g.*, formation of a polymeric surface layer) [36] Despite the large irreversible loss, a high charge (Li$^+$ deintercalation) capacity of ∼900 mAh g^{-1} is still attained in the first cycle. Afterward, the following charge-discharge curves are very similar, implying that the electrochemical reactions proceed into the stable cycling stages.

The charge/discharge capacities *vs.* cycle number at a rate of 0.1 C for urchin-like Co_3O_4 hollow spheres are shown in Fig. 5b. The sample exhibits improved specific capacities over 100 cycles. It is interesting to observe a marked increase in the specific capacities during the initial cycles with the maximum value of ∼1270 mAh g^{-1} during the 48th cycle. Then, the specific capacity gradually decreases to ∼1190 mAh g^{-1} during the 100th cycle. This cycling feature has also been previously observed for mesoporous, nanowire and nanoparticle Co_3O_4 [49]. The capacities exceeding the theoretical value are associated with increased charge storage within the polymeric surface layer [36,49]. On the other hand, not all the surface is covered by the polymer layer during the first discharge since the internal surface of active materials within the pores is more difficult to access. Thus, the polymeric surface layer builds up slowly, over a number of cycles, which results in a marked increase of excess capacity over the first

48 cycles. In comparison, the cycling performances of Co_3O_4 hexapods with sizes of 5–8 μm prepared by $I_{NH_4F:Co(NO_3)_2} = 10 : 1$ was also investigated at 0.1 C. As shown in Fig. 5b, the Co_3O_4 hexapod electrode suffers from rapid capacity fading. The discharge capacities decrease from 988 mAh g^{-1} during the first cycle to 166 mAh g^{-1} during the 100th cycle. Such inferior properties can be attributed to its bulk size without hierarchical structure, which results a long diffusion length for lithium ions transportation from the surface to the centre and the central active materials can not contribute to the capacity.

Good high-C-rate performances are desirable in developing high power/fast charging lithium ion batteries. The performance of Co_3O_4 hollow urchins was also evaluated at high currents (Fig. 5c), *e.g.* from 0.5 to 10 C. The Co_3O_4 hollow urchins show high 2nd-cycle discharge capacities of 878 mAh g^{-1}, 852 mAh g^{-1}, 796 mAh g^{-1}, 695 mAh g^{-1}, 565 mAh g^{-1} and 433 mAh g^{-1} at 1 C, 2 C, 3 C, 5 C, 8 C and 10 C rates, respectively. In contrast, the specific capacities of Co_3O_4 hexapods drop rapidly at increased currents (Fig. 5c). For example, the Co_3O_4 hexapods only show a 2nd-cycle discharge capacity of 184 mAh g^{-1} at 5 C. The rate performance of Co_3O_4 hollow urchins is comparable to some of reported state-of-art electrode, *e.g.*, carbon/Co_3O_4 composite nanospheres showing
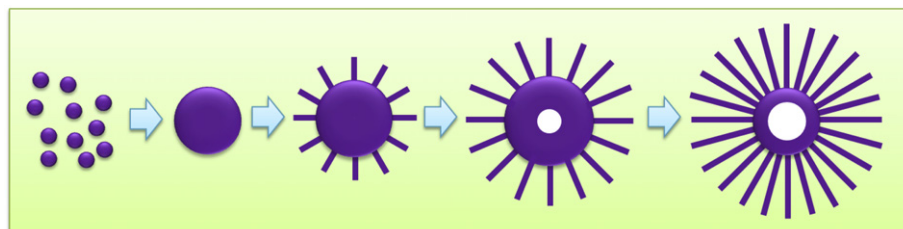

Fig. 3. Schematic illustration of the formation process of the urchin-like $Co(CO_3)_{0.5}(OH)\cdot 0.11H_2O$ hollow spheres.
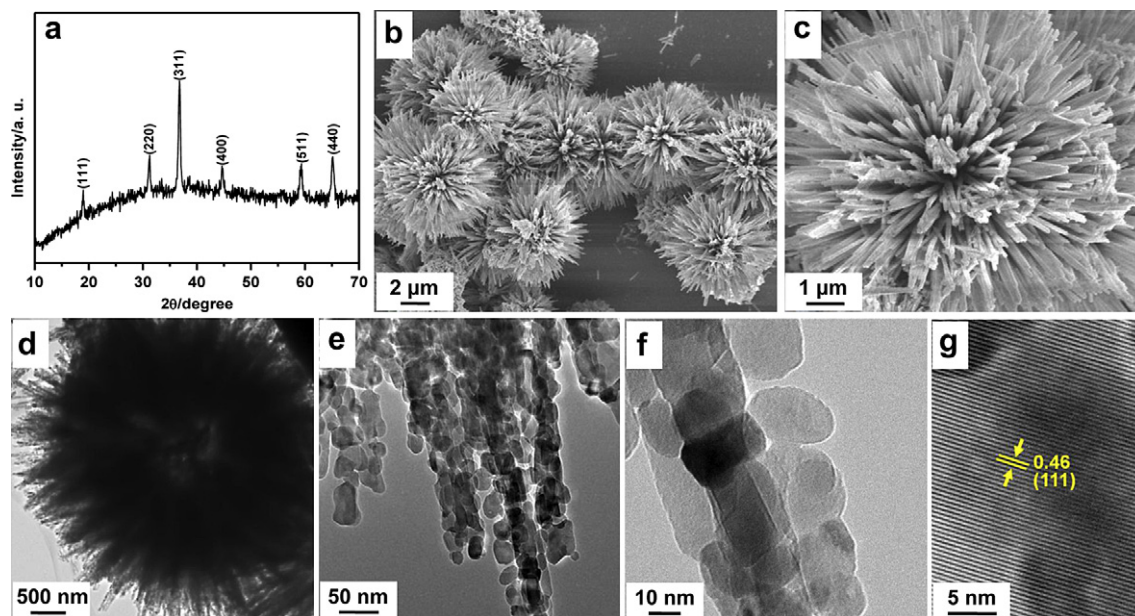
Fig. 4. The XRD pattern (a) and corresponding FESEM images at different magnifications (b, c) for the urchin-like Co_3O_4 spheres prepared through annealing the urchin-like $Co(CO_3)_{0.5}(OH)\cdot0.11H_2O$ precursor in air at 400 °C for 2 h. (d) TEM image of an individual hollow sphere. (e, f) A detailed view of urchin-like Co_3O_4 sphere (TEM images). (g) HRTEM image of a Co_3O_4 nanoparticle.

capacities of ∼400 mAh g^{-1} at 2 C [50], hierarchical porous Co_3O_4 array films delivering capacities of ∼650 mAh g^{-1} at 3 C [51], and Fe_3O_4 nanorods/SWNT electrode exhibiting capacities of ∼800 mAh g^{-1} at 5 C [52].

The impedance analysis was carried out to further understand the good rate performance of the Co_3O_4 hollow urchins. As shown in Fig. 5d, the Co_3O_4 hexapod anode show larger radius of semi-circle in the Nyquist plots as compared to that of Co_3O_4 hollow
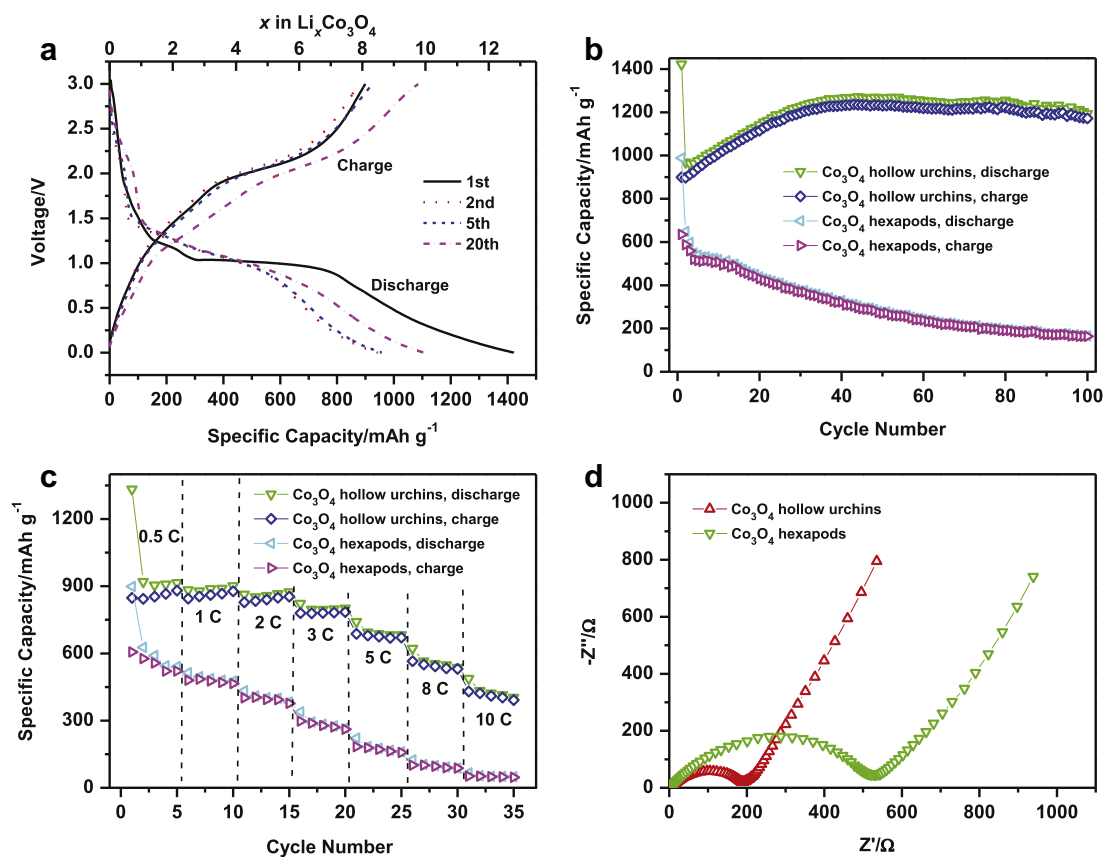

Fig. 5. (a) Galvanostatic charge–discharge voltage profiles of urchin-like Co_3O_4 hollow spheres at a current density of 90 mA g^{-1} (0.1 C). (b) Cycling performances of urchin-like Co_3O_4 hollow spheres and Co_3O_4 hexapods at a rate of 0.1 C. (c) Rate capabilities of the above two anodes at higher current varied from 0.5 C to 10 C. (d) Electrochemical impedance spectra of the above two electrodes measured at the 4th fully discharged state.

urchin electrodes. The smaller radius of the semi-circle indicates lower charge-transfer resistances. The excellent electrochemical performance of Co_3O_4 hollow urchins is believed to result from its unique hierarchical architecture (*i.e.*, nano/microstructure). The nano-sized particles are able to shorten Li^+ diffusion paths. Meanwhile, the void space in the hollow urchin can accommodate the volume change of the active materials during charge/discharge process; also lead to fast infiltration of electrolyte and effective interaction between the electrolytes and active materials.

4. Conclusions

We have developed a simple template-free method for the synthesis of hierarchical urchin-like Co_3O_4 hollow spheres *via* a hydrothermal route followed by a heat treatment process. The growth process of $Co(CO_3)_{0.5}(OH)\cdot 0.11H_2O$ hollow urchin precursors has been investigated and a plausible mechanism is proposed. When tested as the anode materials for LIBs, hierarchical urchin-like Co_3O_4 hollow spheres exhibit high lithium storage capacity, good cycling stability, and superior rate capability (*e.g.*, 433 mAh g^{-1} at 10 C).

Acknowledgments

Appendix A. Supplementary data

Supporting information related to this article can be found at http://dx.doi.org/10.1016/j.jpowsour.2012.08.094.

References

[1] X.W. Lou, D. Deng, J.Y. Lee, J. Feng, L.A. Archer, Adv. Mater. 20 (2008) 258.
[2] Y.G. Li, B. Tan, Y.Y. Wu, Nano Lett. 8 (2008) 265.
[3] W.Y. Li, L.N. Xu, J. Chen, Adv. Funct. Mater. 15 (2005) 851.
[4] J.X. Zhu, Y.K. Sharma, Z.Y. Zeng, X.J. Zhang, M. Srinivasan, S. Mhaisalkar, H. Zhang, H.H. Hng, Q.Y. Yan, J. Phys. Chem. C 115 (2011) 8400.
[5] L. Yang, S. Cheng, Y. Ding, X.B. Zhu, Z.L. Wang, M.L. Liu, Nano Lett. 12 (2012) 321.
[6] H.K. Kim, T.Y. Seong, J.H. Lim, W.I. Cho, Y.S. Yoon, J. Power Sources 102 (2001) 167.
[7] Q. Yang, Z.Y. Lu, Z. Chang, W. Zhu, J.Q. Sun, J.F. Liu, X.M. Sun, X. Duan, RSC Adv. 2 (2012) 1663.
[8] H. Pang, F. Gao, Q. Chen, R.M. Liu, Q.Y. Lu, Dalton Trans. 41 (2012) 5862.
[9] A.M. Cao, J.S. Hu, H.P. Liang, W.G. Song, L.J. Wan, X.L. He, X.G. Gao, S.H. Xia, J. Phys. Chem. B 110 (2006) 15858.
[10] F. Jiao, H. Frei, Angew. Chem. Int. Ed. 48 (2009) 1841.
[11] D.E. Zhang, Q. Xie, A.M. Chen, M.Y. Wang, S.Z. Li, X.B. Zhang, G.Q. Han, A.L. Ying, J.Y. Gong, Z.W. Tong, Solid State Ionics 181 (2010) 1462.
[12] H. Li, G.T. Fei, M. Fang, P. Cui, X.A. Guo, P. Yan, L.D. Zhang, Appl. Surf. Sci. 257 (2011) 6527.
[13] X.H. Xia, J.P. Tu, J. Zhang, X.H. Huang, X.L. Wang, W.K. Zhang, H. Huang, Electrochem. Commun. 10 (2008) 1815.
[14] R. Liu, J. Duay, S.B. Lee, Chem. Commun. 47 (2011) 1384.
[15] A. Magasinski, P. Dixon, B. Hertzberg, A. Kvit, J. Ayala, G. Yushin, Nat. Mater. 9 (2010) 353.
[16] P.G. Bruce, B. Scrosati, J.M. Tarascon, Angew. Chem. Int. Ed. 47 (2008) 2930.
[17] X.L. Wang, W.Q. Han, H.Y. Chen, J.M. Bai, T.A. Tyson, X.Q. Yu, X.J. Wang, X.Q. Yang, J. Am. Chem. Soc. 133 (2011) 20692.
[18] X.H. Rui, D.H. Sim, K.M. Wong, J.X. Zhu, W.L. Liu, C. Xu, H.T. Tan, N. Xiao, H.H. Hng, T.M. Lim, Q.Y. Yan, J. Power Sources 214 (2012) 171.
[19] X.H. Rui, J.X. Zhu, W.L. Liu, H.T. Tan, D.H. Sim, C. Xu, H. Zhang, J. Ma, H.H. Hng, T.M. Lim, Q.Y. Yan, RSC Adv. 1 (2011) 117.
[20] J.X. Zhu, Z.Y. Yin, H. Li, H.T. Tan, C.L. Chow, H. Zhang, H.H. Hng, J. Ma, Q.Y. Yan, Small 7 (2011) 3458.
[21] D.H. Sim, X.H. Rui, J. Chen, H.T. Tan, T.M. Lim, R. Yazami, H.H. Hng, Q.Y. Yan, RSC Adv. 2 (2012) 3630.
[22] Y. Yu, L. Gu, X.Y. Lang, C.B. Zhu, T. Fujita, M.W. Chen, J. Maier, Adv. Mater. 23 (2011) 2443.
[23] Y.L. Ding, J.A. Xie, G.S. Cao, T.J. Zhu, H.M. Yu, X.B. Zhao, Adv. Funct. Mater. 21 (2011) 348.
[24] F.F. Cao, J.W. Deng, S. Xin, H.X. Ji, O.G. Schmidt, L.J. Wan, Y.G. Guo, Adv. Mater. 23 (2011) 4415.
[25] H.L. Wang, L.F. Cui, Y.A. Yang, H.S. Casalongue, J.T. Robinson, Y.Y. Liang, Y. Cui, H.J. Dai, J. Am. Chem. Soc. 132 (2010) 13978.
[26] X.H. Rui, D.H. Sim, C. Xu, W.L. Liu, H.T. Tan, K.M. Wong, H.H. Hng, T.M. Lim, Q.Y. Yan, RSC Adv. 2 (2012) 1174.
[27] X.H. Rui, J.X. Zhu, D. Sim, C. Xu, Y. Zeng, H.H. Hng, T.M. Lim, Q.Y. Yan, Nanoscale 3 (2011) 4752.
[28] F. Wang, J. Yang, Y.N. NuLi, J.L. Wang, J. Power Sources 196 (2011) 4806.
[29] H. Kim, B. Han, J. Choo, J. Cho, Angew. Chem. Int. Ed. 47 (2008) 10151.
[30] X.W. Lou, L.A. Archer, Z.C. Yang, Adv. Mater. 20 (2008) 3987.
[31] T. He, D.R. Chen, X.L. Jiao, Y.L. Wang, Y.Z. Duan, Chem. Mater. 17 (2005) 4023.
[32] X.W. Xie, W.J. Shen, Nanoscale 1 (2009) 50.
[33] E.L. Salabas, A. Rumplecker, F. Kleitz, F. Radu, F. Schuth, Nano Lett. 6 (2006) 2977.
[34] L. Li, Y. Li, S.Y. Gao, N. Koshizaki, J. Mater. Chem. 19 (2009) 8366.
[35] Y.S. Ding, L.P. Xu, C.H. Chen, X.F. Shen, S.L. Suib, J. Phys. Chem. C 112 (2008) 8177.
[36] X. Wang, X.L. Wu, Y.G. Guo, Y.T. Zhong, X.Q. Cao, Y. Ma, J.N. Yao, Adv. Funct. Mater. 20 (2010) 1680.
[37] T. Yu, Y.W. Zhu, X.J. Xu, Z.X. Shen, P. Chen, C.T. Lim, J.T.L. Thong, C.H. Sow, Adv. Mater. 17 (2005) 1595.
[38] L. Fu, Z.M. Liu, Y.Q. Liu, B.X. Han, P.G. Hu, L.C. Cao, D.B. Zhu, Adv. Mater. 17 (2005) 217.
[39] H. Li, G.T. Fei, P. Cui, Y. Jin, X.Y. Feng, C.H. Chen, Chin. J. Chem. Phys. 24 (2011) 343.
[40] Y. Liu, X.G. Zhang, Y. Wu, Mater. Chem. Phys. 128 (2011) 475.
[41] J.M. Ma, A. Manthiram, RSC Adv. 2 (2012) 3187.
[42] X.H. Xia, J.P. Tu, Y.Q. Zhang, Y.J. Mai, X.L. Wang, C.D. Gu, X.B. Zhao, RSC Adv. 2 (2012) 1835.
[43] J. Jiang, J.P. Liu, X.T. Huang, Y.Y. Li, R.M. Ding, X.X. Ji, Y.Y. Hu, Q.B. Chi, Z.H. Zhu, Cryst. Growth Des. 10 (2010) 70.
[44] H. Pan, J.S. Qian, Y.M. Cui, H.X. Xie, X.F. Zhou, J. Mater. Chem. 22 (2012) 6002.
[45] H.K. Wang, F. Fu, F.H. Zhang, H.E. Wang, S.V. Kershaw, J.Q. Xu, S.G. Sun, A.L. Rogach, J. Mater. Chem. 22 (2012) 2140.
[46] Z.Y. Lu, J.X. Zhu, D.H. Sim, W.W. Zhou, W.H. Shi, H.H. Hng, Q.Y. Yan, Chem. Mater. 23 (2011) 5293.
[47] J.X. Zhu, K. Sun, D.H. Sim, C. Xu, H. Zhang, H.H. Hng, Q. Yan, Chem. Commun. 47 (2011) 10383.
[48] S. Saadat, J.X. Zhu, M.M. Shahjamali, S. Maleksaeedi, Y.Y. Tay, B.Y. Tay, H.H. Hng, J. Ma, Q.Y. Yan, Chem. Commun. 47 (2011) 9849.
[49] K.M. Shaju, F. Jiao, A. Debart, P.G. Bruce, Phys. Chem. Chem. Phys. 9 (2007) 1837.
[50] N. Jayaprakash, W.D. Jones, S.S. Moganty, L.A. Archer, J. Power Sources 200 (2012) 53.
[51] X.H. Xia, J.P. Tu, J.Y. Xiang, X.H. Huang, X.L. Wang, X.B. Zhao, J. Power Sources 195 (2010) 2014.
[52] C.M. Ban, Z.C. Wu, D.T. Gillaspie, L. Chen, Y.F. Yan, J.L. Blackburn, A.C. Dillon, Adv. Mater. 22 (2010) E145.